RSC Advances

This is an *Accepted Manuscript*, which has been through the Royal Society of Chemistry peer review process and has been accepted for publication.

Accepted Manuscripts are published online shortly after acceptance, before technical editing, formatting and proof reading. Using this free service, authors can make their results available to the community, in citable form, before we publish the edited article. This *Accepted Manuscript* will be replaced by the edited, formatted and paginated article as soon as this is available.

You can find more information about *Accepted Manuscripts* in the Information for Authors.

Please note that technical editing may introduce minor changes to the text and/or graphics, which may alter content. The journal's standard Terms & Conditions and the Ethical guidelines still apply. In no event shall the Royal Society of Chemistry be held responsible for any errors or omissions in this *Accepted Manuscript* or any consequences arising from the use of any information it contains.

ROYAL SOCIETY OF CHEMISTRY

www.rsc.org/advances

RSC Advances

RSC Publishing

Paper

Structure and Photoluminescence Characteristics of Europium (III) Doped in $CaAl_2Si_2O_8$ Phosphors

Cite this: DOI: 10.1039/xoxxoooooox

W.B. Dai [a,†], M. Zhou [b], Z. Y. Xian [b], L. K. Zeng [b],

Received ooth January 2014,
Accepted ooth January 2014

DOI: 10.1039/xoxxoooooox

www.rsc.org/

A series of Eu^{3+} activated $CaAl_2Si_2O_8$ phosphors have been synthesized at 1350°C under air condition and their photoluminescence properties have been investigated as a function of activator concentrations. The results show that the dominant emission peak of the phosphors $Ca_{1-3x/2}Al_2Si_2O_8$: xEu^{3+} is located at ~611nm due to the Eu^{3+} transition ($^5D_0 \rightarrow {}^7F_2$). The reduction reaction from Eu^{3+} to Eu^{2+} is observed by the luminescent spectra due to the charge compensation mechanism and the special structure of the $CaAl_2Si_2O_8$ host lattice even synthesized in air condition. The energy transfer rate between the Eu^{3+} pairs is not very high that proved by the results of the decay lifetimes and the efficiency of the Eu^{3+} $^5D_0 \rightarrow {}^7F_2$ emissions. The thermal quenching behaviour is attributed to the crossover process from the $^5D_0$ to the charge transfer state (Eu^{3+}-O^{2-}) band. The CIE chromaticity coordinates of the red emission of the $Ca_{0.925}Eu_{0.05}Al_2Si_2O_8$ phosphor is (0.59, 0.28), which is the NTSC system standard for red chromaticity. With enhanced properties (i.e., colour render property) and could be efficient stimulated by NUV and blue UV LEDs, this kind of phosphors can be used in developing novel types of flat panel and projection displays and so on.

1. Introduction

Nowadays, the use of phosphors represents a fast growing industry due to the wide range of applications. [1] As the very important ingredient in phosphors, rare-earth (RE) ions have been playing an important role in modern lighting and display fields because of the abundant emission colours based on its 4f-4f or 5d-4f transitions. [2] Luminescence of Eu^{3+} in complex oxides has been developed for applications in lighting (such as Y_2O_3: Eu^{3+} [3] and YVO_4: Eu^{3+} [4] used in fluorescence lamps) and display (such as Y_2O_2S: Eu^{3+} [5] used in colour television) fields. The knowledge on the 4f-4f transitions of Eu^{3+} in a specific host lattice (HL) makes it possible to estimate the locations of the energy levels for other lanthanide ions in the same site of a certain host. Due to the trivalent lanthanide ions have similar ionic radii, [6] the site occupancy for Eu^{3+} in a given host can be, in some extent, considered as a reference for other lanthanide ions in the same HL. Hence, the studying on the spectroscopic properties of Eu^{3+} in different HL is important not only for fundamental research but also for application.

Oxide phosphors have gained interest due to their better thermal and chemical stability and environmental friendliness compared with sulfides, which are currently used in the screen of flat-panel displays (FPDs), vacuum fluorescent displays (VFDs) and field emission displays (FEDs). [7-12] The acquirement of novel and enhanced properties of new types of flat panel and projection displays has been stimulated a need for development of new oxide optical phosphors. In other word, development of novel phosphors is, therefore, one of the most important aspects in designing luminescent devices. On the other hand, inherent luminescence properties of RE ions are also quite important. It is well-known that Eu^{2+} emits a broad band (4f-5d) which can span in a large wavelength region ranging from ultraviolet to yellow (and even red) depending on the crystal field strength generated by the surrounding ligands, which depends on their charge, size and the strength of the ligand-to-metal ion bond. [13, 14] Eu^{3+} doped materials are also widely investigated. In contrast with Eu^{2+} cations, the emission of Eu^{3+} is made up of narrow lines occurring at longer wavelengths (red or orange luminescence) which, in turn, are very useful for light applications. These emission lines are mainly associated with transitions from the excited $^5D_0$ level to the ground state ^7F_j within the $4f^6$ configuration. [14]

Phosphors with (oxide) aluminosilicates structure have been regarded as effective HLs for luminescent materials. [13, 15] Among the many synthetic aluminosilicates, the anorthite $CaAl_2Si_2O_8$ (CASO) is one of the most used efficient HL for doping various rare-earth (RE) ions. [13, 16] For the different RE^{3+} ions, red luminescence of Eu^{3+} ion is of technological importance. So for, many research groups have involved in studying the fluorescence properties of Eu doped in different HLs, even in the CASO. [17] In this study, the author adopts the solid-state method to synthesis CASO with various Eu^{3+} concentrations and research the structural and luminescence properties of these powder phosphors. The prepared phosphors are potentially applied for UVLED and other devices.

2. Experimental section

2.1. Raw materials and synthesis process

RSC Advances Accepted Manuscript

Powder samples series of phosphors with compositions of $Ca_{1-3x/2}Al_2Si_2O_8$: xEu^{3+} (x = 0.005 to 0.15, except where indicated, all dopant percentage in this study is in mol unit) were prepared through solid-state-reactions. Basically, Calcium carbonate ($CaCO_3$ 99.997% Alfa Aesar), Silica (SiO_2 99.99% Chempur), Alumina-γ (Al_2O_3 99.997% Alfa Aesar), Europium oxide (Eu_2O_3 99.99%), were weighted in the appropriate proportions without further purification. Hereafter, Eu^{3+} doping percentages will refer to an ideal $CaAl_2Si_2O_8$ formula, that is, charge balance of the $CaAl_2Si_2O_8$: Eu x% will correspond for instance to the targeted $Ca_{1-3x/2}Eu_xAl_2Si_2O_8$ composition. Staring materials were ball milled with a Fritsch Pulverisette 7 for two hours in silicon nitride container 70% filled with ethanol. Then, after drying in room temperature, the blends were synthesized at 1350°C for about 50h in alumina crucibles under air atmosphere.

2.2. Structure characterizations

The phase purity and crystal structure of the powder were examined by powder X-ray diffraction (XRD) profiles which were measured with a Bruker AXS D8 advanced automatic diffractometer with Cu K-L_3 radiation (germanium monochromator) operated at 40 kV and 40 mA. Furthermore, the structure refinements based on Gebert's crystal investigations [18] are carried out with the Jana 2006 Beta version software. [19] The instrumental function was expressed in terms of the geometry of the diffractometer with the relevant parameters which reported in Table 1.

Table 1 Instrumental data Used for Rietveld Refinements of CASO and its Eu^{3+}-activated Derivatives

Primary and second radius	217.5 mm
Receiving slit length	16 mm
Glancing angle	13.65º
Source and sample length	12 mm
Primary soller slit aperture	2.5º
Reception slit divergence angle	0.2º
Receiving slit width	0.1 mm
Peak-shape function	Lorentzian

2.3. Optical measurements

The photoluminescence (PL) and PL excitation (PLE) spectra for all the phosphors were obtained with a Spex Fluorolog-3 spectrofluorometer (Instruments Jobin Yvon) equipped with a 450-W Xe light source and double excitation monochromators. The diffuse-reflectance spectra were obtained by a Hitachi U-4100 spectrophotometer with the reflection of black felt (reflection 3%) and white Al_2O_3 (reflection 100%) in the wavelength region of 200-600nm. High temperature (25-200°C) PL was measured by using a heating holder with a thermal coupled and electric heater. In the measurements of time-resolved fluorescence spectra, a 266-nm light generated from the Fourth-Harmonic-Generator pumped by the pulsed Nd: YAG laser was used as excitation source. It was with a line width of 1.0 cm^{-1}, pulse duration of 10 ns, and repetition frequency of 10 Hz.

3. Results and discussion

3.1. Crystal and structural characters

CASO was cataloged to be crystallized in a triclinic crystal system with space group I-1 under ambient pressure by Angel in 1988 [20] which has both layered and framework structure. In the layered structure, the Ca^{2+} ions are located in the interlayers of the double tetrahedral layer and are expected to exchange readily through the interlayers. According to the Wyckoff, CASO structure contains four crystallographically different Ca sites at the same Wyckoff position, 4i (Figure 1).

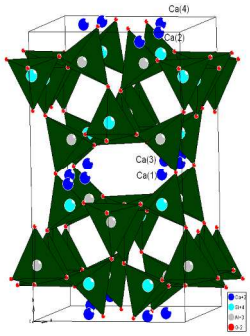

Figure.1 CASO structure represented in cell along the c axic.

The XRD patterns for all the prepared phosphors were collected in the 10-90° 2θ range and all the doped samples diffraction peaks are in good agreement with those reported in JCPDS files 89-1462 (CASO) as exemplified in Figure 2 for x = 0.05. No characteristic peaks of the dopants (Eu^{3+}) were observed after a full pattern matching analysis, which means a solid-state solution is produced in all the samples to be researched. Note here, the experimental spectrum is not fitted well with the calculate spectrum in Figure 2 which can be explained by the following: i) powder diffraction was from CASO structure (triclinic, with lower symmetry) which induce overlap of the diffraction peaks and ii) the different radii between Eu^{3+} and Ca^{2+} made the distort of the bond angle and length and iii) lots of holes would be created in the CASO host lattice for the charge balance and many O^{2-} ions may go into the interval of the lattice also caused the bad refinement induced by the different valence between Eu^{3+} and Ca^{2+} ions. [21, 22]

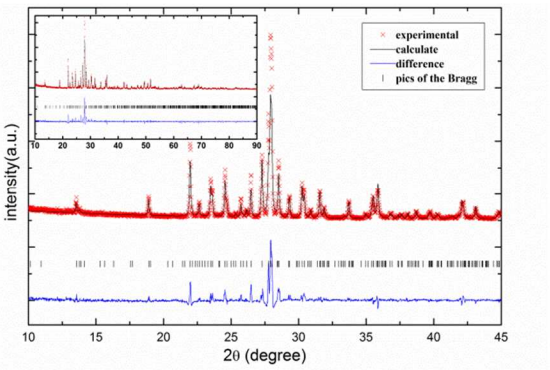

Figure.2 Observed, calculated and difference X-ray diffraction pattern of an Eu^{3+} (0.05)-doped CASO phosphor in the [10-45] 2θ range (inset is given the total pattern).

RSC Advances Accepted Manuscript

This journal is © The Royal Society of Chemistry 2014

The lattice parameters for $C_{0.925}ASO: 0.05Eu^{3+}$ and CASO HL are calculated (based on the experimental XRD profiles with cell refinement software (Jana 2006) by using a Rietveld procedure with the fundamental parameter approach in the I-1 space group) as shown in Table 2 for comparison. The volume of the $C_{0.925}ASO: 0.05Eu^{3+}$ powder was found to be smaller than the un-doped CASO HL due to the radii Eu^{3+} ion smaller than Ca^{2+} ion (Table 2). This is clearly another clue to conclude that the Eu^{3+} ions are doped into the CASO HL.

Table 2 Crystallographic details for $Ca_{0.925}Eu_{0.05}Al_2Si_2O_8$ and CASO HL

Formula	$Ca_{0.925}Eu_{0.05}Al_2Si_2O_8$	CASO HL
Formula weight (g/mol)	2261.36	2263.46
Cryst syst	Anorthic(triclinic)	Anorthic(triclinic)
Space group [1]	I-1	I-1
a (Å)	8.1822(3)	8.2963(2)
b (Å)	12.8743(5)	12.9734(3)
c (Å)	14.1767(5)	14.6484(2)
α (deg)	93.156(3)	93.258(2)
β (deg)	115.736(3)	115.784(4)
γ (deg)	91.207(3)	91.215(2)
V (Å^3)	1341.52(10)	1342.34(20)
Z	8	8
CN	6 and 7	6 and 7
D_{calcd}(g/cm^{-1})	2.7544(2)	2.8534(3)
R_p(%)	7.22	5.43
R_{wp}(%) [2]	3.61	2.63
GOF [3]	1.79	1.58

[1] According to Angel et al, the anorthite form of CASO may crystallize in the I-1 space group. The multiplicity of the Wyckoff sites occupied by calcium cations is doubled compared to P-1 SG but the occupancy rate is about 50%. So far, based on X-ray patterns collected in this study, we couldn't distinguish between the two models and we systematically privileged the I-1 SG.[2] Rwp = weighted profile residual factor. [3] GOF = goodness-of-fit on F^2.

Due to the charge balance, all the four Ca^{2+} sites are not full occupied and induced the disorder of bond angle and length. According to Park et al [23], the broad emission band can only be deconvoluted in two contributions (in room temperature) associated with the occupation of two different chemical sites by RE cations. Namely, one type of Ca^{2+} ion occupies an octahedral site with six oxygen atoms and the average Ca-O bond distance is 2.485 Å. Other Ca^{2+} ions occupy three kinds of polyhedral sites with seven coordinated oxygen atoms and their average bond distances are 2.508, 2.531, and 2.562 Å, respectively (Figure 3). Therefore, it is expected that RE ions doped in this HL will exhibit two kinds of luminescence properties according to their different coordinate number (CN). Al and Si atoms both occupy tetrahedral sites with three coordinated oxygen atoms, and the average bond distances for Al-O and Si-O are 1.735 and 1.611 Å, respectively. Based on the effective ionic radii (r) of cations with different CN reported by Shannon, [24] it can be proposed that Eu^{3+} ions are expected to occupy the Ca^{2+} sites preferably. Because the ionic radii (Pauling's) of Eu^{3+} (r = 0.947 Å when CN = 6, r = 1.05 Å when CN = 7) is much closer to that of Ca^{2+} (r = 1.00 Å when CN = 6, r = 1.06 Å when CN = 7). Since both four coordinated Al^{3+} (r = 0.39 Å) and Si^{4+} (r = 0.26 Å) sites are too small for Eu^{3+} to occupy.

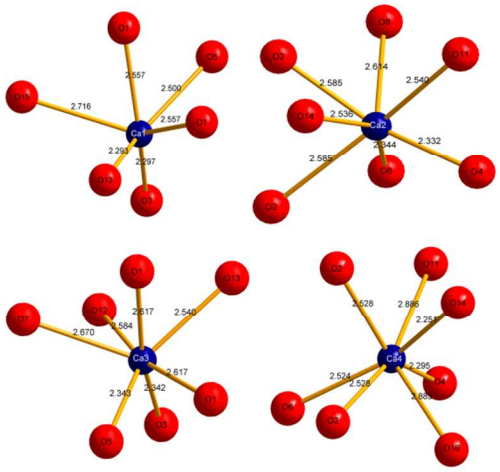

Figure.3 Calcium environments and bond length in CASO HL (Wyck.: 4i).

3.2. Optical properties of phosphors $C_{1-3x/2}ASO: xEu^{3+}$

Figure 4a shows the diffuse reflection spectra relationship between the CASO HL and $C_{0.925}ASO: 0.05Eu^{3+}$. Obviously, with the Eu^{3+} doped in the CASO, when compared with the HL, the onset of the absorption of the doped Eu^{3+} band extends to a long-wavelength side from 388 nm to 576 nm. Meanwhile, the absorption intensity is quite enhanced in the whole area especially in the blue area, which perfectly matches with the emission of the blue-InGaN based LEDs. The HL has the broad absorption band from 200nm to 388nm, which is attributed to the Ca^{2+}-O^{2-} group and the absorption edge at 388nm (3.20ev). [25, 26] Compared with the HL, the absorption spectrum of the doped CASO consists of two parts: one is a broadband from 200nm to 263nm assigned to the Eu^{3+}-O^{2-} charge transfer band (CTB), another is sharp peaks in the range from 350nm to 600nm that are associated with typical intra-4f forbidden transitions of the Eu^{3+}. The energy of the lower CT absorption depends on the electronegativity difference between the Eu^{3+}-O^{2-} ligand and the Ca^{2+}-O^{2-}. The longer wavelength of the edge of the absorption spectrum is caused by the smaller electronegativity Eu^{3+}-O^{2-} compared to the Ca^{2+}-O^{2-}. [27-29] Figure 4b shows the PLE spectra for the $C_{1-3x/2}ASO: xEu^{3+}$ samples sintered at different concentration of Eu^{3+} ions, by monitoring the emission wavelength at 611nm ($^5D_0 \rightarrow {}^7F_2$). In Eu^{3+} doped phosphors, the intensity of the CTB is stronger than that of the f-f transitions due to the probability of the electron transitions of the state band (O^{2-}) is larger than the intra-

RSC Advances Accepted Manuscript

configurational f-f transitions. [30] The PLE spectra reveal the broad excitation peaks overlapped with CTB in the shorter wavelength region, and it also consists of sharp excitation bands in the longer wavelength area due to the f-f transitions of Eu^{3+} ions. The CTB which may affect the thermal quenching [25, 28, 29] is due to the charge transfer between the completely filled 2p orbital of O^{2-} ion and the partially filled 4f orbital of the Eu^{3+} ion and the position of this band depends strongly on the HL. There are a series of sharp excitation bands present between 360nm and 580nm that are associated with the typical intra-4f transition of the Eu^{3+} ions that centered at 361, 382, 393, 413, 464, 530 and 576nm were attributed to the $^7F_0 \rightarrow {}^5D_4$, $^7F_0 \rightarrow {}^5L_7$, $^7F_0 \rightarrow {}^5L_6$, $^7F_0 \rightarrow {}^5D_3$, $^7F_0 \rightarrow {}^5D_2$, $^7F_0 \rightarrow {}^5D_1$ and $^7F_0 \rightarrow {}^5D_0$ transitions, respectively, which is agreed with the result of Figure 4(a). We can see clearly from the excitation spectra, the dominated excitation is located at ~393nm. Meanwhile, the 393nm (strongest excitation peaks) means the $C_{1-3x/2}ASO: xEu^{3+}$ phosphor is quite suitable to be used for near-UV exciting red phosphor for display devices.

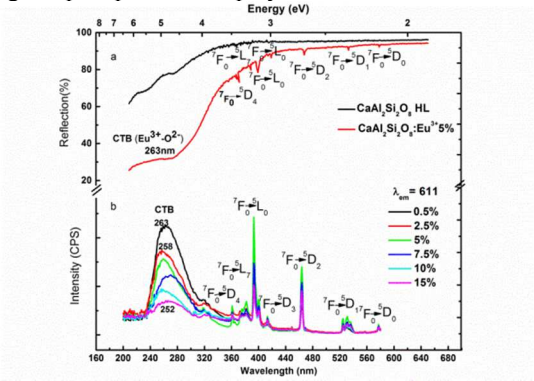

Figure.4 (a) Diffuse reflection spectra of undoped (black line) and 5% Eu^{3+}-doped CASO and (b), excitation spectra of $C_{1-3x/2}ASO: xEu^{3+}$ (x = 0.5% to15%).

It is worthy to note that the intensities of CTB at ~263nm shift towards the higher energy side which indicates that the quantum efficiency of Eu^{3+} increases with increasing the Eu^{3+} concentration (Figure 4b). The CTB is associated with the stability of the electron of the surrounding O^{2-} ion and this is the reason why the CT transition is very sensitive to a ligand environment (i.e., the bonding energy between the central ion and the ligand ions, namely, the strong potential energy field between the anion sites (O^{2-}) and the surrounding cation ions). [27, 30, 31] If this potential increases, the energy required for transferring an electron from the O^{2-} ion to the cation (Eu^{3+}) increases too. Hence, the CTB moves to higher energy side. This also means that the mixing of Eu^{3+} and O^{2-} orbitals decreases, as a result the intensity of the CTB decrease. [30] This is the case in this study because: i) the average radii Eu^{3+} is smaller than Ca^{2+}, when the Eu^{3+} ions substitute the Ca^{2+} sites, the Eu^{3+}-O^{2-} distance, in average, will become shorter following the volume of the unit cell decreases as the Eu^{3+} ions concentration increases, and this result can indicate that Eu-O bonds become stronger and more covalent and less ionicity, strengthening the binding energy of an electron to O^{2-}. Therefore, the electron needs more energy to transfer from O^{2-} to Eu^{3+}, resulting in the CTB shifts slightly to higher energy and decreases the intensity. It need also be noted that following the Eu^{3+} doped concentration increases, the excitation intensities originated from the Eu^{3+} will increase at first and then decrease, this phenomenon might be associated with an appearance of Eu^{3+}-Eu^{3+} pairs in the HL because of the decrease in the average distance between Eu^{3+} ions, and the energy will likely transfer between Eu^{3+}-Eu^{3+} ions and so decrease the intensity of excitation spectrum. ii) There are two different crystallographically Ca^{2+} sites in the structure of CASO HL corresponding to the different coordination, namely, 6- and 7-, respectively. When the Eu^{3+} ions substitute the Ca^{2+} sites, one can image that the probability of the tendency to occupy the different Ca^{2+} sites is different (explained by Pauling's second rule). [32] Each ion should be approximately equal to its oxidation state. This statement can be expressed by the following relation: $V_i = n \times S_{ij}$, Where V_i is the oxidation state of the ion, n equal to the number of coordination and S_{ij} is the sum of the valences of its bonds. The electrostatic strength of each Ca site was calculated by this equation. Clearly, using the equation above, the 6- and 7- coordinated Ca site are about +0.3333 and +0.2857, respectively. Thus, the low 6-coordination Ca site will have a high electrostatic strength than the 7-'s. Thus, the Eu^{3+} ions would more likely to substituting the low coordination site which has a large electrostatic strength (and this will also influence the thermal stability, discussed later). Because the Eu^{3+} ions are more likely to occupying the low coordination 6-Ca site, as we already know that the average radii of the Ca^{2+} (6- coordination)-O^{2-} is smaller than the 7-'s radii of the Ca^{2+}-O^{2-}. Thus, the rate of the decreasing of the average radii of the Eu^{3+}-O^{2-} will higher in the beginning than later for the higher Eu^{3+} concentration. Because following doped more Eu^{3+} ions, the Eu^{3+} ions will no doubt to occupied the 7- coordinated sites. Therefore, it was the reason why the CTB change a lot especially in the lower concentration of the Eu^{3+}. As for the PLE spectra in the longer wavelength (from 360 nm to 580 nn), the intensities decrease following Eu^{3+} dopant concentrations (exceed 5%) is due to the energy transfer (concentration quenching) between Eu^{3+}-Eu^{3+} pairs.

Figure 5 shows the emission spectra of $C_{1-3x/2}ASO: xEu^{3+}$ with different Eu^{3+} concentrations under λ_{ex} = 393 nm ($^7F_0 \rightarrow {}^5L_6$). Obviously, these phosphors can be excited with the intense f-f transition at 393nm and CTB (because of the overlap between the CTB and typical intra-4f forbidden transitions of the Eu^{3+}). In any cases, this indicates that these phosphors can strongly absorb NUV light and transfer to the red radiation. The strongest emission peak of each phosphor located at 611nm, which is attributed to the transition of $^5D_0 \rightarrow {}^7F_2$. The moderate other emission bands at 582-602, 675-710 and 739-766nm are assigned to the $^5D_0 \rightarrow {}^7F_1$, $^5D_0 \rightarrow {}^7F_3$ and $^5D_0 \rightarrow {}^7F_4$ transitions of the Eu^{3+} ions, respectively. Generally, the ^7F_J energy levels of Eu^{3+} also split into some components under crystal field effects caused by surrounding ions. [25, 30] Under the lower symmetry of the Eu^{3+} ions sites, $^7F_1$ and $^7F_2$ split into three and five components, respectively, according to completely lifted [2J+1] degeneracy, if overlapping of higher ^5D_J emission can be excluded, though they cannot be with completely certainty. In this case, the emission at 574 and 578nm (Figure 6) due to $^5D_0 \rightarrow {}^7F_0$ are particularly noted. Since the splitting of either $^5D_0$ and $^7F_0$ is not possible, the presence of two peaks must be due to separate emission from the two different sites occupied by the Eu^{3+} in the CASO structure, namely, Eu^{3+} (CN = 6) and Eu^{3+} (CN = 7), respectively. Typically, these peaks always very weak or even altogether absent. But in this case here, both sites in this structure have low symmetry, which can be readily to relax the selection rules. [33, 34] The different Ca^{2+} (Eu^{3+}) sites explained why there are shoulder peaks on one broad peak in figure 6. The line shape of emission does not change following the different Eu^{3+} ions concentrations doped in CASO HL due

RSC Advances Accepted Manuscript

This journal is © The Royal Society of Chemistry 2014

to electronic transitions within the non-bonding $4f^6$ shell of Eu^{3+}. As a consequence, $\Delta R = 0$ (in configurational coordinate diagram, R is the metal-ligand distance, structural parameter) yielding narrow lines. [14] Meanwhile, the concentration quenching can be observed when the doping rate at ~ 5% as shown in Figure 5(a).

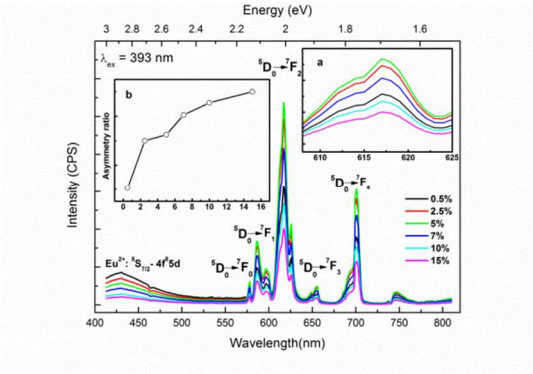

Figure.5 Emission spectra of $C_{1-3x/2}ASO: xEu^{3+}$ phosphors under λ_{ex} = 393 nm, inset (a) shows the emission spectra range from 608 nm to 625nm for the transition of $^5D_0$ to $^7F_2$ vs. Eu^{3+} concentrations and inset (b), shows dependence of the asymmetry ratio on Eu^{3+} ions concentrations.

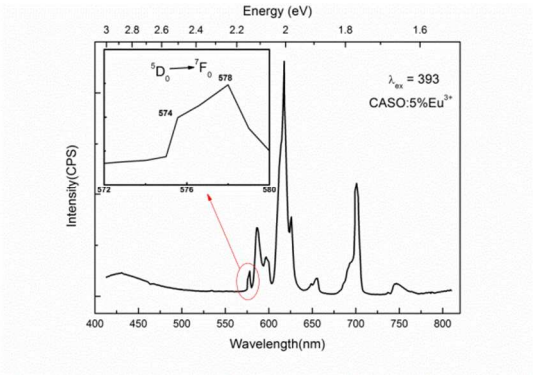

Figure.6 PL of Eu^{3+} (5%) doped in CASO. The inset shows the enlarged the range of the emission from the transition $^5D_0 \rightarrow {}^7F_0$.

Note here, a few transitions are sensitive to the environment and these have been called hypersensitive transitions. In this study, the electric dipole transition $^5D_0 \rightarrow {}^7F_2$ is such kind of hypersensitive. When the Eu^{3+} ions are located at a low symmetry site, the $^5D_0 \rightarrow {}^7F_2$ emission transition often dominates in the emission spectrum. According to the Judd-Ofelt theory, [35] the magnetic dipole $^5D_0 \rightarrow {}^7F_1$ transition is regardless of environment. In Eu^{3+} ions doped in CASO phosphors, the emission intensity of $^5D_0 \rightarrow {}^7F_2$ is stronger than the emission intensity $^5D_0 \rightarrow {}^7F_1$, which indicates the Eu^{3+} ions have lower inversion center. Meanwhile, the $(^5D_0 \rightarrow {}^7F_2)/(^5D_0 \rightarrow {}^7F_1)$ emission intensities ratio (asymmetry ratio) can be used as an index to measure the site symmetry around the Eu^{3+} ions in the CASO HL. [25, 30] Generally, larger the intensity ratio of $^5D_0 \rightarrow {}^7F_2$ to $^5D_0 \rightarrow {}^7F_1$, lower the local symmetry. Figure 5(b) shows the dependence of the $(^5D_0 \rightarrow {}^7F_2)/(^5D_0 \rightarrow {}^7F_1)$ emission intensity ratio on different Eu^{3+} ions concentration. The asymmetric ratio increases slightly with increasing Eu^{3+} concentration, this may due to the decrease of the crystallite size with increasing the Eu^{3+} concentration ($r(Eu^{3+}) < r(Ca^{2+})$), as doping concentration increases, the lattice parameters would be decreased. This confirms the decrease in local symmetry and hence an increase in red emission ($^5D_0 \rightarrow {}^7F_2$ at ~611nm). The lack of an inversion center around the Eu^{3+} ion can provide a high color purity and brightness red phosphor. [25]

The concentration quenching of the Eu^{3+} ions doped in CASO HL can be elucidated by the following two factors: i) the distance between adjacent Eu^{3+} ions decreases with the increasing of doping concentration, the excitation energy transfer due to resonance between the Eu^{3+} ions was enhanced when the doping concentration was increased especially more than 5% in this case here, thus, the excitation energy reaches quenching centers and ii), the activators are paired or coagulated and the excitation energy transfer between them to become the quenching center. The above results suggest that the physical and chemical properties of $C_{1-3x/2}ASO: xEu^{3+}$ phosphors are quite stable even the phosphors sintered at 1350°C for 50h and the optimum concentration of Eu^{3+} is ~ 5%. Although all the phosphors are synthesized in the air condition, still there are exiting some Eu^{2+} ions in the CASO (Figure 5), this phenomenon was also noticed by zhang. [36] The reduction reaction from Eu^{3+} to Eu^{2+} can be explained by the charge compensation mechanism and the special structure of CASO HL (three dimensional networks composed by AlO_4 and SiO_4 tetrahedra which can play a role of shield for Eu^{2+} against from oxidation during the annealing process in air). Thus, the peaks located at about 421nm are no doubt due to the Eu^{2+} $4f^65d^1 \rightarrow 4f^7$ transition as a normally emission band. [26] Meanwhile, we can notice that following the increasing Eu^{3+} concentration, however, the intensity of the Eu^{2+} emissions are monotonous decreased, the reason may be due to: i) the condense of the volume following the Eu^{3+} concentration and hence changer the local structure (band length and band angle) which made the reduction process more difficult and ii), the Eu^{2+} emission band is overlap with the Eu^{3+} excitation band, and following the doped Eu^{3+} ions increasing, the concentration of the Eu^{2+} ions would not be really increased due to phosphor synthesized in air. Hence, energy transfer rate from Eu^{2+} to Eu^{3+} would increase and induce the intensity of Eu^{2+} emission decreasing. In order to support the energy transfer between Eu^{2+} and Eu^{3+}, we measured the decay curves for all samples $C_{1-3x/2}ASO: xEu^{3+}$ (x = 0.5% to 15%) with various *x* as displayed in Figure 7 (under λ_{ex} = 320 and λ_{em} = 420 nm). With the increase of the doping concentration, the decay time of the Eu^{2+} center clearly shortens. This confirms that the energy transfer rate from Eu^{2+} to Eu^{3+} increases with the Eu doping concentration. For all investigated samples, there are not long afterglow can be perceptible with naked eyes, and the fluorescence is white-pink in agreement with the major presence of Eu^{3+}.

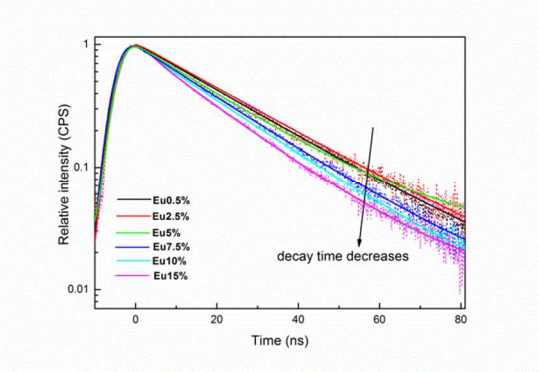

RSC Advances Accepted Manuscript

Figure.7 PL decay curves of Eu^{2+} in $C_{1-3x/2}ASO$: xEu^{3+} (x = 0.5% to 15%) phosphors displayed on a logarithmic intensity scale (excited at 320 nm and monitored at 420 nm).

Furthermore, considerable emission spectra were not clearly observed from the higher $^5D_{3,2,1}$ levels in the shorter wavelength range of 400-550nm (if has, the peaks should be sharp). This is ascribed to the fact that the smaller energy gaps between $^5D_{3,2,1}$ to $^5D_0$ can be bridged by the vibration energies of the silicate and alumina groups present in the CASO HL.[25] This can be explained by the non-radiative process, the excitation energy from the Eu^{3+} ion decaying from a higher excited state $^5D_{3,2,1}$ could promotes a nearly Eu^{3+} ions from the ground state to the metastable state level, such as $^5D_1(Eu_1) + {}^7F_0(Eu_2) \rightarrow {}^5D_0(Eu_1) + {}^7F_3(Eu_2)$. [25, 30] This also can be explained by the fact that: as the concentration of luminescent optical centers (Eu^{3+}) increases, the distance between optical centers becomes small enough to allow a resonant energy transfer, so the energy can be easily transfer from one luminescent center to another. As a result, if Eu^{3+} ion concentration are sufficiently high, the higher level $^5D_{3,2,1}$ emission can be easily quenched via cross relaxation and the $^5D_0$ emission becomes dominant, and this is true in this case. Under the same consideration, at low Eu^{3+} doping concentration, the cross relaxation can be neglected. The intensity of the higher excited state $^5D_{3,2,1}$ emission is very weak compared with that of very low phonon energy host materials. The non-radiation multi-phonon relaxation rate of the $4f^n$ configuration is given by: [35] $W_{NR} = W_{NR}(0)\exp(\alpha n\hbar\omega_p)$. Where α depends on the character of the phonon, W_{NR} is the relaxation rate, ΔE is the energy difference between the levels, $\hbar\omega_p$ is the highest available vibrational phonon energy, and $n = \Delta E/\hbar\omega_p$ is the number of phonon to fill the energy gap. According to the equation, a higher maximum available phonon energy can reduce the number of phonons and thus fill the energy gap and enhance multiphonon relaxation to bridge the energy level between $^5D_{3,2,1}$ and $^5D_0$. Hence, the $^5D_{3,2,1}$ emission intensity of CASO:Eu^{3+} is very weak compared with that of $^5D_0$ emissions.

The decay lifetimes (τ, as shown in Figure 8, for $x < 0.05$, the decay curves are more suitable for fitting by a single-exponential function while $x \geqslant 0.05$, curves better fitted by a double-exponential function) for the donor ions Eu^{3+} in the CASO HL would be affected by the energy transfer process between Eu^{3+}-Eu^{3+} pairs and can be expressed by: [34] $1/\tau = 1/\tau_0 + P_t$, where τ_0 is the lifetime for the donor ions when missing the acceptor and P_t is the average probability of transfer to the energy sink in the HL. [26] In some extent, we can define that the decay time ($^5D_0 \rightarrow {}^7F_2$) for the lowest doping concentration in this case (0.5% percentage of Eu^{3+} in CASO HL) is the τ_0 which means that the quantum efficiency is equal to 100% (at this case, τ_0 = 1.56 ms). Meanwhile, the reduction of the efficiency of the energy from the Eu^{3+}-Eu^{3+} pairs to the energy sink (P_t) can be introduced by: [37] $\eta = (1/\tau_0)/(1/\tau)$. As listed in Table 3, the reduction of the efficiency is only reached to ~ 22% in the CASO HL. Based on the efficiency and the decay lifetimes for different doping concentrations, the energy transfer between Eu^{3+} pairs is considerably not very strong which may due to the connection of the Eu^{3+} ions were shielded in the structure of the CASO HL.

Table 3 Distance between the dopants Eu^{3+}, decay times (τ) monitored at $^5D_0 \rightarrow {}^7F_2$ transition and efficiency (η) for the different concentrations of Eu^{3+}

x (= Eu^{3+} dopant concentration)	τ (decay time, ms)	η (efficiency)
0.5%	1.56	-
2.5%	1.51	96.79%
5%	1.45	92.95%
7%	1.37	87.82%
10%	1.31	83.97%
15%	1.22	78.21%

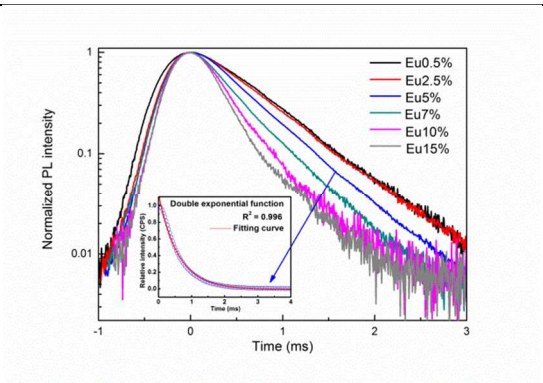

Figure.8 PL decay curves of Eu^{3+} in $C_{1-3x/2}ASO$: xEu^{3+} (x = 0.5% to 15%) phosphors displayed on a logarithmic intensity scale (under λ_{ex} = 393 and λ_{em} = 611). Inset displays the fitting curve for x = 0.05 (fitted by double-exponential function). The average values (τ) are listed in Table 3.

3.3. Thermal quench behaviour of ^5D_j

Figure 9 shows the thermal stability of phosphor $C_{0.925}ASO$: $0.05Eu^{3+}$ from the room temperature (25°C) to 200°C. The relative peak intensity of $C_{0.925}ASO$: $0.05Eu^{3+}$ is decreasing (Figure 9(a)) following the increasing of temperature and fell down to 57% about the initial intensity at about 200°C. The absorption of the CASO:Eu^{3+} as shown in Figure 4 indicated a lower Eu^{3+}-O^{2-} CTS band, and thus the lower lying O^{2-} to Eu^{3+} CTB could provide a pathway to relaxation of the excited state via a non-radiative process. Many studies have examined the thermal quenching mechanism of $^5D_0 \rightarrow {}^7F_2$ emission, [25, 30] which can cross over the $^5D_0$ state to the CTS band. The crossover quenching from the $^5D_0$ excited state to the CTB is a thermal activation process that can be described by: [38] $I(T) = I_0[1+A\exp(-E/KT)]^{-1}$. Where A is a constant and E is the relaxation energy from the $^5D_0$ state to the CTB. The activation energy for thermal quenching of $C_{0.925}ASO$: $0.05Eu^{3+}$ can be obtained by $\ln[I/I(T)]$ versus $1/KT$, as shown in Figure 9(b), and the activation energy is equal to 0.2724 eV ($2194cm^{-1}$). The crossover mechanism is a possible pathway for the thermal quenching, comparing with the multiphonon model that requires 16.3 phonons at $1000cm^{-1}$ to bridge the energy between the $^5D_0$ and $^7F_2$ levels and therefore, is too difficult to obtain. [30]

RSC Advances Accepted Manuscript

This journal is © The Royal Society of Chemistry 2014

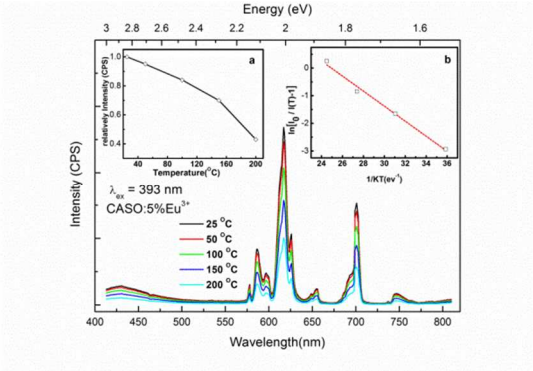

Figure.9 Temperature dependence of emission spectra for $Ca_{0.925}Eu_{0.05}ASO$, the inset (a) shows the relative intensity emission of $Ca_{0.925}Eu_{0.05}ASO$ as a function of temperature and inset (b) plot of relaxation energy for thermal quenching of $Ca_{0.925}Eu_{0.05}ASO$.

According to the absorption spectra and the temperature dependence PL spectra, possible pathways for thermal quenching are presented in Figure 10. The $^5D_3$, $^5D_2$ and $^5D_1$ are relaxed by multiphonon emission or cross-relaxation to the $^5D_0$ state. The pathway of the thermal quenching of the $^5D_0$ state is through a Eu^{3+}-O^{2-} CTS band. Some electrons then overcome the relaxation energy assisted by phonons as the temperature increases and feed to the ^7F_J state, which provides the non-radiative process, and the remaining electrons are contributed to the $^5D_0 \rightarrow {}^7F_1$ emission.

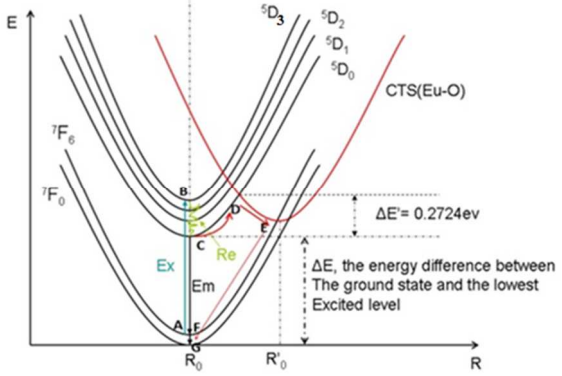

Figure.10 Configurational coordinate diagram for the thermal quenching of the $^5D_0$ state through a CTB. After the absorption transition A → B, the system reaches high vibrational levels of the excited state, subsequently it relaxes to the lowest vibrational level (C point), from where through multiphonon emission or cross-relaxation to the $^5D_0$ state (D point). From D → E, E → F and F → G, the process indicates a nonradiative transition which quenches the luminescence at higher temperature.

3.4. CIE chromaticity of phosphors $C_{1-3x/2}ASO: xEu^{3+}$

The commission International De I-Eclairage (CIE) chromaticity coordinates for $C_{1-3x/2}ASO: xEu^{3+}$ phosphors at different concentrations were calculated and shown in the Figure 11. The CIE chromaticity coordinates of optimized concentration is the point 3 (0.59, 0.28), which is the NTSC system standard for red chromaticity. [39, 40] It is clearly that this serials of phosphors exhibit excellent CIE coordinates which sited in the reddish colour area. There are two key factors that are considered as the reason for controlling the position of the $C_{1-3x/2}ASO: xEu^{3+}$ phosphors in the CIE diagram: i), the asymmetric ratio increases with increasing the Eu^{3+} concentration in the host lattice and ii), the varied intensities of the emission band following the dopant concentrations. Based on these considerations, it is useful as a red phosphor for the production of artificial white light to be similar to those of natural white light owing to its better spectral overlap. All these results can give a way to application of $C_{1-3x/2}ASO: xEu^{3+}$ phosphor to be used in the NUV-LEDs as well as optical display systems.

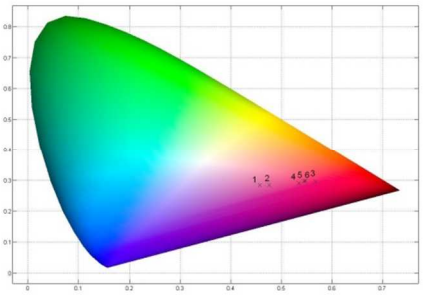

Figure.11 Evolution of CIE Chromaticity coordinates for $C_{1-3x/2}ASO: xEu^{3+}$, point 1 to 6 corresponding to the concentration of Eu^{3+} from 0.5% to 15%, repectively.

Conclusions

In summary, through the ceramic synthesis process, the pure phases of the aluminosilicates phosphors $C_{1-3x/2}ASO: xEu^{3+}$ were obtained and their optical properties were investigated. This serial of phosphors can be excited through a large range from the near-UV to blue LEDs when used in solid-state lighting field. The local environment surrounding Eu^{3+} ions have lower inversion center in the CASO HL due to the the asymmetry ratio increases following the dopant concentrations. There exists energy transfer between the dopant ions (Eu^{3+}-Eu^{3+} pairs) and the critical concentration is at ~5%. Although synthesized in air condition, all phosphors still exist a trace of Eu^{2+} ions as confirmed by the PL spectra due to the charge compensation mechanism and the special structure of the CASO HL. Because of the crossover quenching between the Eu^{3+} $^5D_0$ energy level of the excited state and the CTB (Eu^{3+}-O^{2-}), the thermal quenching were also observed. All these phenomena can give us an incentive to think about using of this series of phosphors in the NUV-LEDs or UV-LEDs as well as optical display systems.

Acknowledgements

The author acknowledges S. Jobic, P. Deniard, H. Brault and F. Massuyeau for the technical assistance and fruitful discussion in IMN, Nantes University, CNRS, FRANCE. This work has been supported by the Chinese Scholarship Council (CSC), NO: 2009615018.

Notes and references

[a] State Key Laboratory of Luminescent Materials, South China University of Technology

[b] School of Materials Science and Engineering, South China University of Technology

† Corresponding author, E-mail: wubin.dai@foxmail.com, fax: + 86 20 87 11 02 73.

RSC Advances Accepted Manuscript

1. X. Liu, C. Li, Z. Quan, Z. Cheng and J. Lin, *J. Phys. Chem. B*, 2007, 111, 16601-16607.
2. P. Dorenbos, *J. Lumin.*, 2000, 91, 155-176.
3. T. S. Atabaev, O. S. Jin, J. H. Lee, D.-W. Han, H. H. T. Vu, Y.-H. Hwang and H.-K. Kim, *RSC Adv.*, 2012, 2, 9495-9501.
4. Q. Luo, S. Shen, G. Lu, X. Xiao, D. Mao and Y. Wang, *RSC Adv.*, 2012, 2, 616-621.
5. J. Dhanaraj, R. Jagannathan and D. C. Trivedi, *J. Mater. Chem.*, 2003, 13, 1778-1782.
6. C. Liu, H. Liang, X. Kuang, J. Zhong, S. Sun and Y. Tao, *Inorg. Chem.*, 2012, 51, 8802-8809.
7. A. Vadivel Murugan, A. K. Viswanath, V. Ravi, B. A. Kakade and V. Saaminathan, *Appl. Phys. Lett.*, 2006, 89, 123120.
8. Y. Shimomura and N. Kijima, *J. Electrochem. Soc.*, 2004, 151, H86-H92.
9. F.-L. Zhang, S. Yang, C. Stoffers, J. Penczek, P. N. Yocom, D. Zaremba, B. K. Wagner and C. J. Summers, *Appl. Phys. Lett.*, 1998, 72, 2226-2228.
10. S. Y. Seo, K.-S. Sohn, H. D. Park and S. Lee, *J. Electrochem. Soc.*, 2002, 149, H12-H18.
11. S. S. Yi, J. S. Bae, B. K. Moon, J. H. Jeong and J. H. Kim, *Appl. Phys. Lett.*, 2005, 86, 071921.
12. J. Y. Cho, Y. R. Do and Y.-D. Huh, *Appl. Phys. Lett.*, 2006, 89, 131915.
13. F. Clabau, A. Garcia, P. Bonville, D. Gonbeau, T. Le Mercier, P. Deniard and S. Jobic, *J. Solid State Chem.*, 2008, 181, 1456-1461.
14. G. Bless and B. C. Grabmaire, *Luminescent Materials*, Springer Verlag, Berlin, 1994.
15. M. Gaft, H. Yeates, L. Nagli and G. Panczer, *J. Lumin.*, 2013, 137, 43-53.
16. L. Zhang, C.-N. Xu, H. Yamada and N. Bu, *J. Electrochem. Soc.*, 2010, 157, J50-J53.
17. X. Yu, X. H. Xu, T. M. Jiang, H. L. Yu, P. H. Yang, Q. Jiao, J. B. Qiu, *J. Mater. Chem. Phys.*, 2013, 139, 314-318.
18. W. Z. Gebert, *Kristallogr*, 1972, 135, 437.
19. V. D. Petricek and M. L. Palatinus, *The Crystallographic Computing System JANA, 2006 Beta*, Academy of Sciences: Praha, Czeck Republic, 2006.
20. R. J. Angel, *Am. Mineral.*, 1988, 73, 1114.
21. W. B. Dai, J. Mater. Chem. C, (2013), DOI: 10.1039/c3tc32378a.
22. W. B. Dai, RSC Adv., 2014, 4, 11206-11215.
23. J. K. Park, J. M. Kim, E. S. Oh and C. H. Kim, *Electrochem. Solid St.*, 2005, 8, H6-H8.
24. R. D. Shannon, *Acta Crystallogr*, 1976, A32, 751.
25. Y.-C. Chang, C.-H. Liang, S.-A. Yan and Y.-S. Chang, *J. Phys. Chem. C*, 2010, 114, 3645-3652.
26. W.-J. Yang, L. Luo, T.-M. Chen and N.-S. Wang, *Chem. Mater.*, 2005, 17, 3883-3888.
27. X. Qiao and H. J. Seo, *Mater. Res. Bull.*, 2014, 49, 76-82.
28. C. K. Jørgensen, *Coord. Chem*, 1994, 21, 226.
29. C. Pe´drini, *Phys. Status Solidi A*, 2005, 202, 185-194.
30. S. Zhang, Y. Huang, L. Shi, X. Qiao and H. J. Seo, *Phys. B: Condens. Matter*, 2009, 404, 4136-4141.
31. X. Qiao and H. J. Seo, *J. Alloy. Compd.*, 2013, 578, 188-194.
32. Z. S. Herman, in *Theoretical and Computational Chemistry*, eds. Z. B. Maksić and W. J. Orville-Thomas, Elsevier, 1999, vol. Volume 6, pp. 701-748.
33. A. J. Moad and G. J. Simpson, *J. Phys. Chem. B*, 2004, 108, 3548-3562.
34. S. F. Wong and G. J. Schulz, *Phys. Rev. Lett.*, 1975, 35, 1429-1432.
35. S. Y. Shionoya, W. M., *Phosphor handbook*, CRC Press: Boca Raton, FL,, 1999.
36. C. Zhang, J. Yang, C. Lin, C. Li and J. Lin, *J. Solid State Chem.*, 2009, 182, 1673-1678.
37. J. B. Garcı´a Sole´, L. E.; Jaque, D., *An Introduction to the Optical Spectroscopy of Inorganic Solids;*, Wiley & Sons, Ltd.: Chichester, U.K., 2005.
38. W. H. Fonger and C. W. Struck, *J. Chem. Phys.*, 1970, 52, 6364-6372.
39. M. Sugasawa and K. Yamamoto, Google Patents, 1991.
40. Y. Faroudja and J. Roizen, *Smpte J.*, 1987, 96, 750-761.

RSC Advances Accepted Manuscript

 This journal is © The Royal Society of Chemistry 2014